crystals

MDPI

Article

First-Principles Study of MoS_2, WS_2, and NbS_2 Quantum Dots: Electronic Properties and Hydrogen Evolution Reaction

Omar H. Abd-Elkader [1,*], Hazem Abdelsalam [2,3], Mahmoud A. S. Sakr [4], Abdallah A. Shaltout [5] and Qinfang Zhang [2,*]

1 Department of Physics and Astronomy, College of Science, King Saud University, P.O. Box 2455, Riyadh 11451, Saudi Arabia
2 School of Materials Science and Engineering, Yancheng Institute of Technology, Yancheng 224051, China
3 Theoretical Physics Department, National Research Centre, El Buhouth Str., Dokki, Cairo 12622, Egypt
4 Basic Science Department, Faculty of Engineering, Misr University of Science and Technology (MUST), 26th of July Corridor, Al Motamayez District, 6th October City 12566, Egypt
5 Spectroscopy Department, Physics Research Institute, National Research Centre, El Behooth Str., Dokki, Cairo 12622, Egypt
* Correspondence: omabdelkader7@ksu.edu.sa (O.H.A.-E.); qfangzhang@ycit.edu.cn (Q.Z.)

Abstract: The electronic and catalytic properties of two-dimensional MoS_2, WS_2, and NbS_2 quantum dots are investigated using density functional theory investigations. The stability of the considered structures is confirmed by the positive binding energies and the real vibrational frequencies in the infrared spectra. The ab initio molecular dynamics simulations show that these nanodots are thermally stable at 300 K with negligible changes in the potential energy and metal–S bonds. The pristine nanodots are semiconductors with energy gaps ranging from 2.6 to 3 eV. Edge sulfuration significantly decreases the energy gap of MoS_2 and WS_2 to 1.85 and 0.75 eV, respectively. The decrease is a result of the evolution of low-energy molecular orbitals by the passivating S-atoms. The energy gap of NbS_2 is not affected, which could be due to the spin doublet state. Molecular electrostatic potentials reveal that the edge sulfur/transition metal atoms are electrophilic/nucleophilic sites, while the surface atoms are almost neutral sites. MoS_2 quantum dots show an interestingly low change in the hydrogen adsorption free energy ~0.007 eV, which makes them competitive for hydrogen evolution catalysts.

Keywords: MoS_2; WS_2; and NbS_2; quantum dots; DFT; electronic properties; hydrogen evolution reaction

check for updates

Citation: Abd-Elkader, O.H.; Abdelsalam, H.; Sakr, M.A.S.; Shaltout, A.A.; Zhang, Q. First-Principles Study of MoS_2, WS_2, and NbS_2 Quantum Dots: Electronic Properties and Hydrogen Evolution Reaction. *Crystals* **2023**, *13*, 994. https://doi.org/10.3390/cryst13070994

Academic Editor: Igor Yurkevich

Received: 5 June 2023
Revised: 17 June 2023
Accepted: 20 June 2023
Published: 21 June 2023

Copyright: © 2023 by the authors. Licensee MDPI, Basel, Switzerland. This article is an open access article distributed under the terms and conditions of the Creative Commons Attribution (CC BY) license (https://creativecommons.org/licenses/by/4.0/).

1. Introduction

Two-dimensional (2D) materials have gained significant interest from researchers in different fields, including physics, chemistry, and material science, due to their exceptional physical and chemical properties [1–3]. The exceptional properties of 2D materials open doors for applications in different fields, including energy storage and conversion [4–7], electronic devices [8–10], gas sensors [11,12], water treatment [13–15], and catalysts [16,17]. An important class of two-dimensional materials is the 2D transition metal dichalcogenides (TMDs). They are described as MX_2, where M is the transition metal (such as Mo, W, or Nb) and X is the chalcogen (S, Se, or Te). TMDs are semiconductors with strong spin-orbit coupling [18,19], an intercalatable layered structure [20], enhanced light absorption [21,22], and strong photoluminance [23,24]. Thus, single-layer MoS_2, with its semiconducting direct band gap of ~1.8 eV and high mobility of 200 $cm^2\ V^{-1}\ s^{-1}$, is applicable for building two-dimensional transistors. Radisavljevic et al. demonstrated a two-dimensional transistor based on monolayer MoS_2 with mobility equal to at least 200 $cm^2\ V^{-1}\ s^{-1}$, comparable to that of graphene nanoribbons, on/off current ratios of 1×10^8 at room temperature, and very low standby power dissipation [25]. Moreover, the challenging fabrication of

nanodevices with gate lengths sub-1 nm has been achieved in vertical MoS_2 transistors with an atomically thin channel and a gate length below 1-nm [26].

Concerning catalysis, two-dimensional TMDs show exceptional catalytic performance due to their high surface area, easy surface functionalization, and abundant active sites [27–30]. Two-dimensional TMDs presented significantly improved catalytic performance compared to their bulk counterparts [31]. For instance, Tian et al. fabricated a few layers of WS_2 nanosheets using lithium-ion intercalation and demonstrated enhancement of the electrocatalytic hydrogen evolution performance with respect to their bulk WS_2 [32]. This enhancement, with a low overpotential of 320 mV at 10 mA cm^{-2}, is mainly a result of the increased number of active sites in the ultrathin WS_2 nanosheets. Compared to other materials, TMDs have the following privileges: (a) they are highly photosensitive and have a suitable band gap for water splitting; (b) they are characterized by low recombination of the photogenerated carriers when compared to current photocatalysts; (c) they have a high light absorption coefficient and many active sites required for performant photocatalysts; and (d) compared to rare earth elements, they are earth-abundant and cost-effective materials [33–35]. It was demonstrated that the edge sites in MoS_2 quantum dots are catalytically active sites for the hydrogen evolution reaction (HER) [36–38]. The main reason for the boosted catalytic properties in quantum dots is the reduction of the size to the quantum regime, where the effect of edges and quantum confinement becomes dominant [39–42]. For instance, it has been reported theoretically and experimentally that the S-atoms at the edges of MoS_2 nanodots are the active sites for HER [36,43]. Based on these results, many researchers have developed highly dispersed MoS_2 quantum dots with sufficient active edges to improve HER performance [44–47]. On the other hand, Hu et al. reported that sulfur vacancies in MoS_2 are active sites for CO_2 dissociation to surface-bound CO and O, hence facilitating the hydrogenation of CO_2 to methanol [48]. Both the experimental and theoretical investigations indicated that the sulfur vacancies at the surface boost the CO_2 hydrogenation to methanol through the inhibition of hydrogenolysis to methane, while the sulfur vacancies at the edges are selective to hydrogenation to methane. This catalyst also showed high stability for more than 3000 h without deterioration in activation or selectivity. Therefore, it is highly important for efficient HER and, in general, for enhanced catalytic performance to identify and study the active sites suitable for the required catalytic reaction and how to enrich them [49,50].

In this work, we apply density functional theory to investigate the electronic properties and HER catalytic performance of three TMD quantum dots, namely MoS_2, WS_2, and NbS_2. We found that the considered TMD quantum dots are semiconductors with energy gaps ranging from 2.6 eV to 3 eV. Edge passivation with sulfur atoms leads to a considerable decrease in the energy gap; for example, the energy gap of MoS_2 decreases from 3 eV to 1.85 eV by edge sulfuration. Therefore, in the current systems, the electronic properties can be controlled not only by the quantum size effect but also by edge functionalization. It is worth noting that several methods have been developed for the synthesis of two-dimensional TMD quantum dots with definite size and edge morphology, including liquid exfoliation [51], lithium intercalation [52], hydrothermal synthesis [53], and chemical vapor deposition [54]. Zhou et al. reported the successful synthesis of WS_2 quantum dots with a defect-free and uniform size of 5 nm using a combination of grinding and sonication techniques [55]. Further sulfuration was applied to decrease the number of defects and improve the conductivity. Thus, the pristine edges and the sulfurated edges considered in this work can be achieved experimentally using the aforementioned sulfuration process. Chemical functionalization to improve the physical and chemical properties of 2D nanostructures has also been demonstrated, such as by attaching sulfur-containing groups to MoS_2 nanosheets [56,57]. Moreover, Tadi et al. reported a single-step method to synthesize MoS_2 quantum dots doped with metals (Fe, Mg, and Li) and studied the effect of doping on boosting the electrocatalytic properties [58]. The calculations of the change in the free energy show that MoS_2 quantum dots have the best HER catalytic performance with a lower free energy change down to 0.007 eV on S-atoms compared to other nanodots.

The paper is organized as follows: the computational model is given in Section 2. The obtained results and their discussion are given in Section 3, and finally, in Section 4, we give our conclusion.

2. Computational Model

The density functional theory (DFT) calculations are performed based on localized functionals as implemented in Gaussian 16 [59]. The selected structures were fully optimized by minimizing the energy by setting the self-consistent field (SCF) conversion criterion to 10^{-4}. The selected functional is the hybrid M06-2X functional due to its wide applicability [60,61]. The effective core potential LANL2DZ basis set is employed in our calculations due to its good performance for transition metals [62,63].

3. Results and Discussion

The considered two-dimensional nanostructures are hexagonal nanodots with armchair edge terminations from MoS_2, WS_2, and NbS_2, as shown in Figure 1. We considered two cases of edge passivation: (a) the pristine case (Figure 1a,c,e) and the passivation of transition metals at the edges with S-atoms (Figure 1b,d,f). The total number of atoms in the pristine case is 63 and increases to 72 after edge passivation with sulfur. The optimized structures shown in Figure 1 imply that passivation of the edge transition metals significantly decreases the deformations at the edges that are observed in the unpassivated structures.

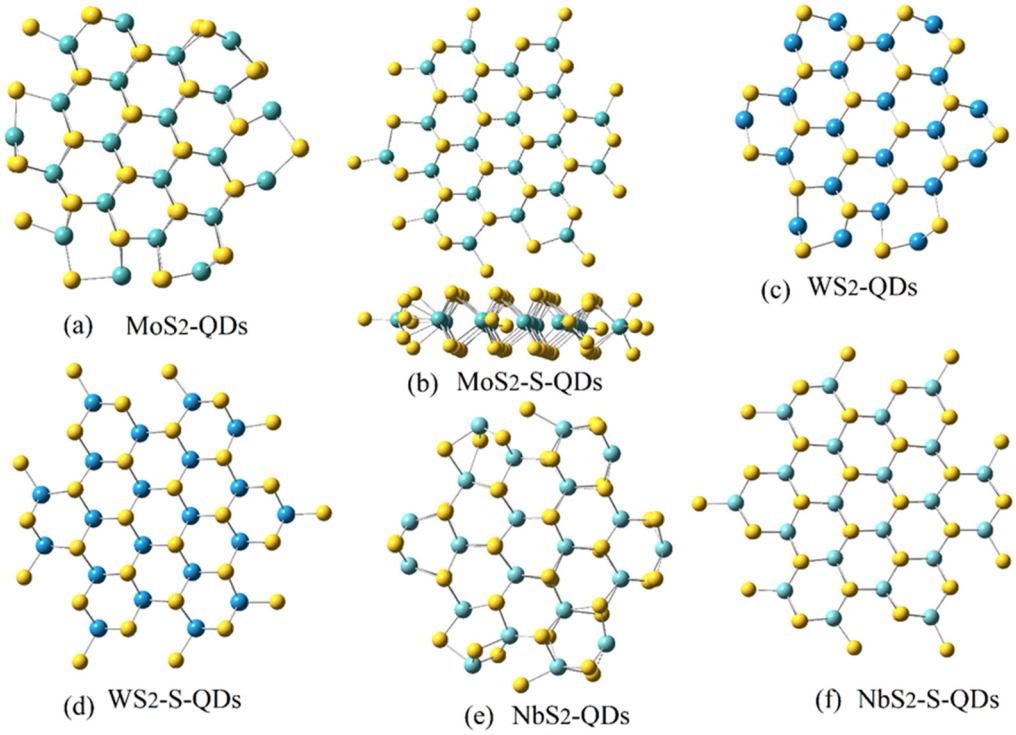


Figure 1. Optimized structures of MoS_2, WS_2, and NbS_2 quantum dots with pristine (**a**,**c**,**e**) and sulfurated (**b**,**d**,**f**) edges.

3.1. Stability

The structural stability of the selected TMD quantum dots has been tested by two methods: (a) calculating the binding energy (E_b) and (b) performing frequency calculations and plotting the infrared (IR) spectra. The binding energy is calculated from $E_b = (n_x E_x + n_s E_s - E_t)/n$, where n_x is the number of the x transition metal atoms (Mo, W, or Nb), n_s is the number of S atoms, and n is the total number of atoms. The corresponding energies are E_x, E_s, and E_t, respectively. The considered nanodots have E_b values ranging from 5.6 to 5.9 eV, with an E_b order of $MoS_2 > WS_2 > NbS_2$. These positive values of E_b

ensure the stable formation of the considered 2D-TMD nanodots. In addition to E_b, we performed frequency calculations from which the IR spectra are obtained. It is observed from the IR spectra, shown in Figure A1, Appendix A, that all the vibrational frequencies are real, with no negative or imaginary frequencies that cause time divergence of the vibration amplitudes. Consequently, the square of the frequency is positive, indicating a minimum on the potential energy surface, and the structures are then geometrically stable.

In addition to the structure stability, the thermal stability is also investigated using ab initio molecular dynamics simulations for all the considered quantum dots at a temperature equal to 300 K. The molecular dynamics simulations are performed using the atom-centered density matrix propagation (ADMP) model [64,65]. The changes in the potential energy and the transition metal-sulfur bond length are simulated for 5 femtoseconds at 300 K, as shown in Figures A2 and A3 in Appendix B. The results show that the changes in the potential energy and the bond length are very small, which confirms the thermal stability of the considered nanodots at 300 K.

3.2. Electronic Properties

Here we study the electronic properties by evaluating the partial density of states (PDOS), the energy gap, and the highest occupied/lowest unoccupied molecular orbitals (HOMO/LUMO) for the selected quantum dots. Quantum stability chemical parameters, such as dipole moment, chemical potential, electronegativity (χ), and molecular electrostatic potentials, are also investigated.

3.2.1. Partial Density of States

From the partial density of states, shown in Figure 2, we can obtain the electronic energy gap, the participation of the constituting atoms (such as Mo and S atoms in MoS_2) in the total density of states, and the change in the density of electronic states by edge passivation. PDOS is calculated using the GaussSum 3 software [66] based on the output files from Gaussian 16. The electronic energy gap of the pristine MoS_2-QDs shown in Figure 1a equals ~3 eV. This wide semiconductor energy gap decreases to 1.85 eV with edge passivation with sulfur. The same is observed in the WS_2 quantum dot with a higher decrease in the energy gap, where the wide energy gap of 2.6 eV decreases to 0.75 eV after edge sulfuration, as seen in Figure 2c,d. Thus, edge modification provides a convenient tool to tune the electronic properties of TMD quantum dots.

The low-energy red peak in Figure 2a, representing the HOMO of MoS_2-QDs, is mainly contributed by Mo atoms. Electronic states from Mo (+4) are expected to participate more in the unfilled molecular orbitals because they acquire negative charges from S (-2) atoms. Thus, the special case of HOMO in Figure 2a is expected to be a result of the bonding between Mo atoms at the edges. Passivation of these edge Mo atoms with S breaks the Mo-Mo bonds, and the new HOMO is mainly contributed by S atoms, as seen in Figure 2b. It is also observed that after passivation, the unoccupied molecular orbitals shift to lower energies, which is the reason for the decrease in the energy gap. This explanation is confirmed by the HOMO/LUMO distributions shown in Figure 3a,b. Where the HOMO distributes on the edge Mo atoms in the first case and on the sulfur atoms in the second case. The contribution to the HOMO by sulfur atoms increases in WS_2- and NbS_2-QDs, as seen in Figure 2c,e. Thus, the HOMO distributions on S-atoms increase, especially in NbS_2 (Figure 3c,e). After edge sulfuration, the HOMO of both WS_2 and NbS_2 is dominated by electrons from sulfur atoms. In WS_2-QDs, the HOMO shifts to higher energies that decrease the energy gap to 0.75 eV. On the other hand, the energy gap of NbS_2 slightly increases with edge sulfuration instead of decreasing as observed in the previous two cases. This effect could be a result of the broken symmetry between the spin-up and spin-down molecular orbitals, where both NbS_2 and NbS_2-S QDs have spin doublet states.

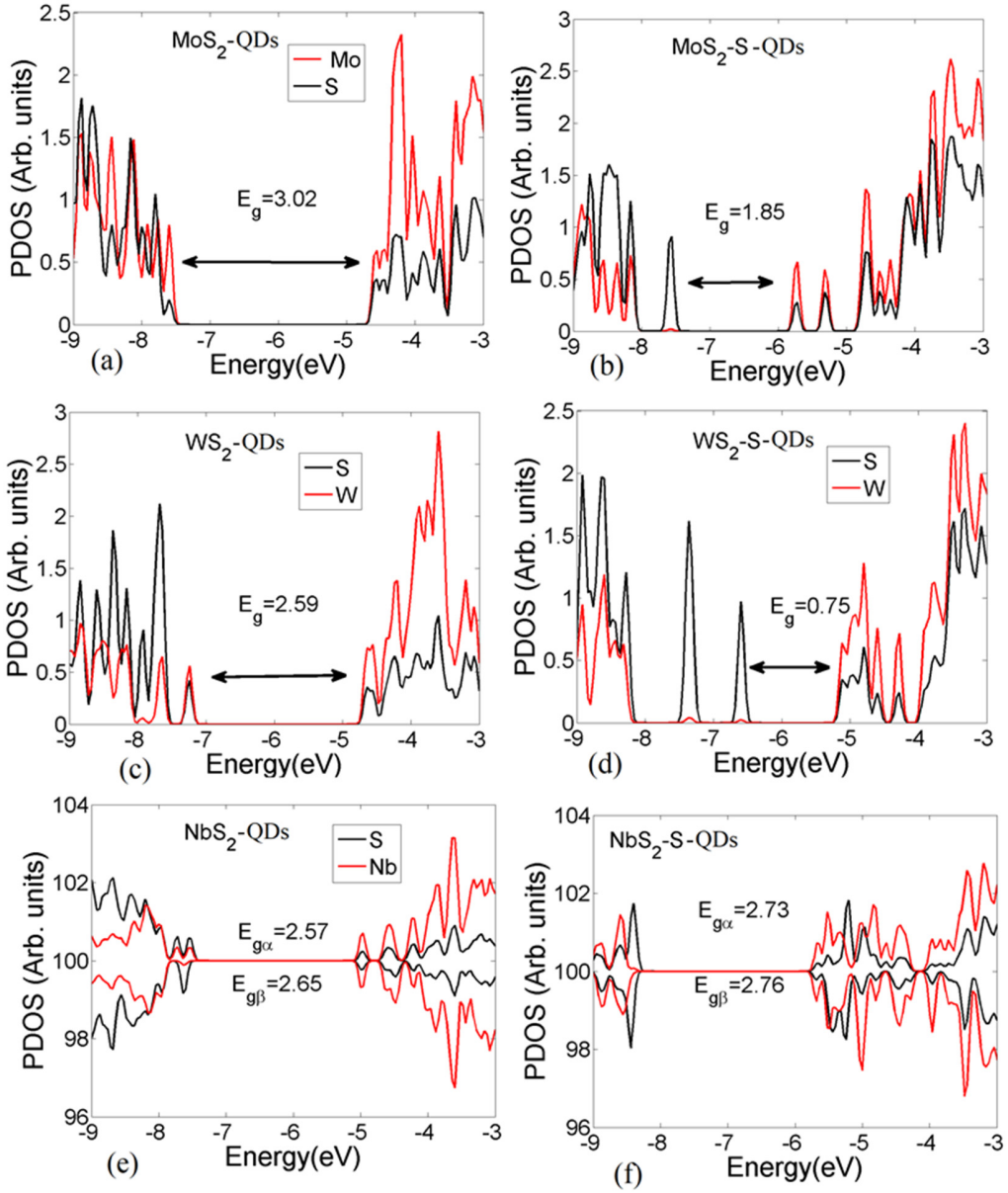


Figure 2. The partial density of states of MoS_2 (**a**), WS_2 (**c**), and NbS_2 (**e**) quantum dots in the unpassivated case and the case of edge passivation with sulfur (**b**,**d**,**f**).

3.2.2. Quantum Stability Chemical Parameters

Considerable quantum stability chemical (QSC) parameters like dipole moment (μ), chemical potential (ρ), electronegativity (χ), and chemical hardness (η) were calculated employing E_{LUMO} and E_{HOMO} values. These QSC parameters are calculated by utilizing the subsequent equations $\rho = \frac{E_{HOMO}+E_{LUMO}}{2}$, $\chi = -\frac{E_HOMO+E_{LUMO}}{2}$, and $\eta = \frac{E_{LUMO}-E_{HOMO}}{2}$. Noteworthy, when a structure has a high μ; it has an important asymmetry in the electronic charge distribution. As presented in Table 1, the μ magnitude of the WS_2-S-QDs is the highest compared to other structures. Therefore, the intramolecular charge transfer in WS_2-S-QDs is more active than in the other structures. As written in Table 1, the ρ value of MoS_2-S-QDs is lower than other studied systems. Those results indicate the escaping electrons from MoS_2-S-QDs are low, contrasting with the other QDs under the current study. On the other side, MoS_2-S-QDs have the highest value of χ and, thus, the highest ability to attract electrons compared to other molecular structures. Furthermore, the chemical hardness value for MoS_2-QDs is large, contrasting with the rest of the other structures. This

means that MoS_2-QDs are undeniably challenging to free electrons, while MoS_2-QDs have extraordinary chances to offer electrons to another acceptor compound.

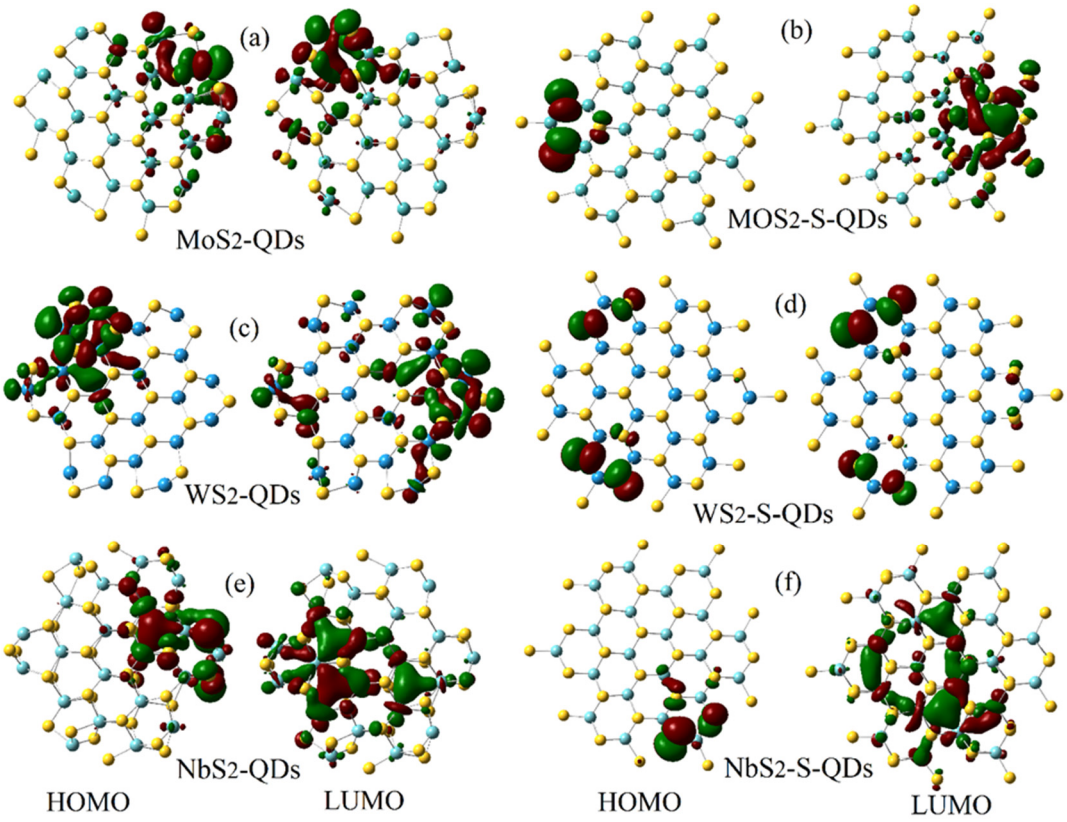


Figure 3. The highest occupied molecular orbital (HOMO) and lowest unoccupied molecular orbital (LUMO) of MoS_2 (**a**), WS_2 (**c**), and NbS_2 (**e**) quantum dots in the pristine case and the case of edge passivation with sulfur (**b**,**d**,**f**).

Table 1. Some important quantum stability chemical (QSC) parameters using the DFT/M06-2X/LANL2DZ method in the gaseous phase.

Nomenclature	L (eV)	H (eV)	P (eV)	X (eV)	H (eV)	μ (D)
MoS_2-QDs	−4.562	−7.580	−6.071	6.071	1.509	2.256
MoS_2-S-QDs	−7.563	−7.610	−7.586	7.586	0.0235	3.219
NbS_2-QDs	−4.960	−7.528	−6.244	6.244	1.284	5.603
NbS_2-S-QDs	−5.642	−8.372	−7.007	7.007	1.365	2.980
WS_2-QDs	−4.636	−7.234	−5.935	5.935	1.299	2.558
WS_2-S-QDs	−6.575	−7.325	−6.950	6.950	0.375	8.268

3.2.3. Molecular Electrostatic Potentials

The electrophilic versus nucleophilic sites of the MoS_2, WS_2, and NbS_2 quantum dots and their sulfur-passivated compounds (MoS_2-S, WS_2-S, and NbS_2-S) are revealed by Molecular Electrostatic Potential (MEP) investigations, which is useful for the prediction of the reaction site. In Figure 4, the MEPs are displayed. Red, blue, and green colors are used to symbolize the negative, positive, and neutral sites at MEP interfaces (See Figure 4). For MoS_2, WS_2, and NbS_2 quantum dots and their sulfur passivated compounds (MoS_2-S, WS_2-S, and NbS_2-S), the negative region (red color) is concentrated around sulfur atoms, indicating that such sites are electrophilic assaults. The terminal Mo, W, and Nb atoms were covered by the positive (blue) zone for MoS_2, WS_2, NbS_2 QDs, and their sulfur passivated compounds (MoS_2-S, WS_2-S, and NbS_2-S), indicating that nucleophilic attack is possible in

these sites. The parts of the molecule that lack any charge distribution are known as the neutral regions (green color).

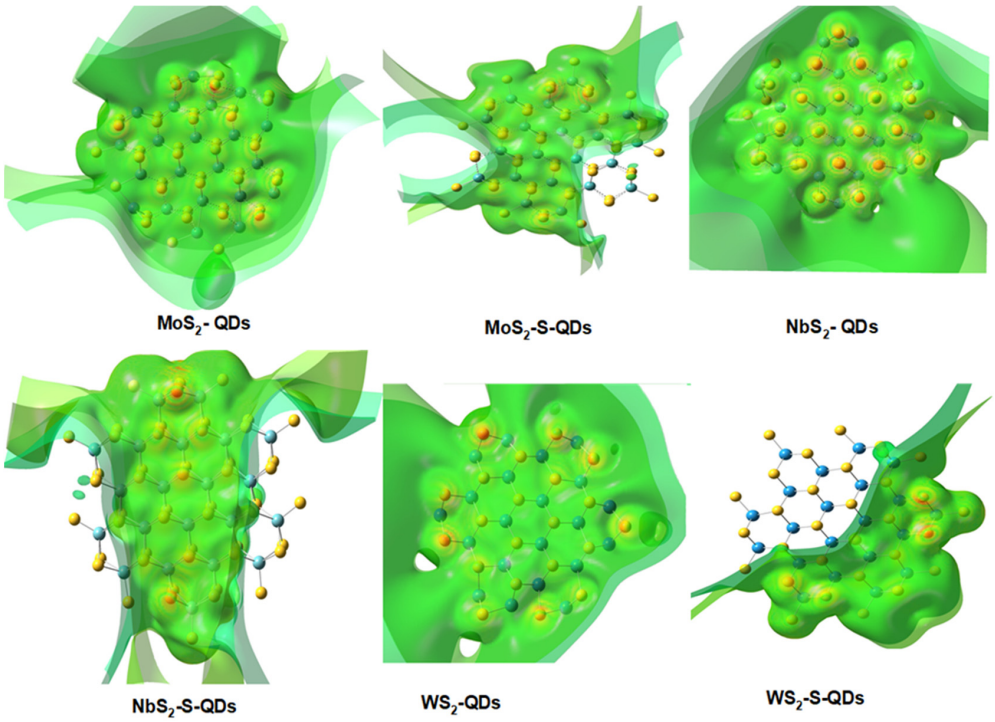


Figure 4. Electrostatic potential map (ESP) for MoS_2, WS_2, NbS_2 quantum dots, and their sulfur passivated compounds (MoS_2-S, WS_2-S, and NbS_2-S).

3.3. Hydrogen Evolution Reaction

To identify the active sites for the hydrogen evolution reaction on the considered structures, different adsorption sites were selected, as shown in Figure 5a. Sites 1 and 2 represent the hydrogen adsorption on the Mo and S atoms at the edges, respectively, while the adsorption on the surface is considered in sites 3 and 4. In the initial structure, the hydrogen atom is located at 2 (Å) above the selected sites. Figure 5b shows the optimized structures of MoS_2-H-3 and MoS_2-H-4, where in both sites the hydrogen atom prefers to interact with the surface sulfur atom. In the case of MoS_2-S, we consider only two sites that are expected to give different results from the selected sites in the pristine case; the first is on the passivating S-atom at the edge, and the second is the S-atom at site 3. We focus on the catalytic performance of only MoS_2 quantum dots because we tested the other nanodots and found that their hydrogen adsorption is higher than that of MoS_2, resulting in lower catalytic activity for the hydrogen evolution reaction.

The following reaction represents the hydrogen evolution reaction in alkaline and neutral solutions:

$$* + H_2O + e^- \rightarrow H^* + OH^- \quad (1)$$

$$H^* + H^* \rightarrow 2^* + H_2 \quad (2)$$

where * represents the catalyst on which hydrogen will be adsorbed and H^* is the catalyst after the adsorption of hydrogen on the selected sites. The first reaction is a result of the oxygen evolution on the other electrode; thus, we focus only on the second reaction. The change in the free energy of the reaction (ΔG) is a good indicator of the efficiency of the hydrogen evolution reaction, where a low value of ΔG means a high catalytic performance toward hydrogen evolution. The calculated values of ΔG for MoS_2 and MoS_2-S QDs are given in Table 2. It is observed that ΔG for all the adsorption sites is very high, up to ~5 eV for site one, except for sites three and four, which represent adsorption on the surface.

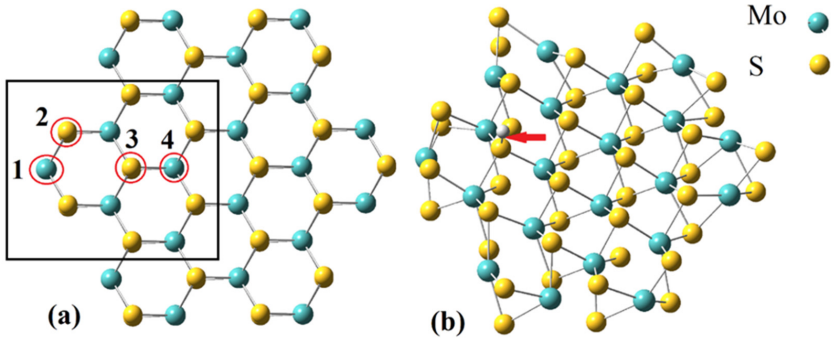


Figure 5. (**a**,**b**) The selected sites on which hydrogen evolution reactions are tested for MoS_2-quantum dots.

Table 2. The change in the free energy (ΔG) for the hydrogen adsorption on different sites represents the hydrogen evolution reaction on the edge and the surface.

Struct.	ΔG (eV)	Struct.	ΔG (eV)
MoS_2-H-1	4.89	MoS_2-H-4	0.007
MoS_2-H-2	3.69	MoS_2-S-H-1	1.74
MoS_2-H-3	0.007	MoS_2-S-H-2	1.74

The reason for the high value of ΔG is the strong interaction between the hydrogen atom and Mo or S atoms at the edges. For instance, a sulfur atom at the edges (at site two in Figure 5a) is connected to two Mo atoms, while a sulfur atom at the surface (at site three) is connected to three Mo atoms. Thus, hydrogen will form a stronger bond with the S-atom in the former case than in the latter, which in turn makes ΔG higher for HER at the edges. On the other hand, ΔG = 0.007 eV for HER on the surface, at sites 3 and 4, which makes MoS_2-QDs promising catalysts for HER. This value of ΔG is lower than that found in hBN- and graphene QDs [67,68]. In addition to the theoretical results presented here, experimental results also showed that the free energy of hydrogen bonding to MoS_2 nanodots is lower than that in metal-free electrocatalysts such as graphene and hBN [69]. It is even low enough to make MoS_2-QDs a promising competitor to the benchmarked but expensive Pt-Catalysts [70].

4. Conclusions

The electronic properties and hydrogen evolution reaction catalytic performances of MoS_2, WS_2, and NbS_2 quantum dots have been investigated using density functional theory calculations. The structural stability of the considered quantum dots is confirmed by the positive binding energy that indicates the stable formation of the structures and the real vibrational frequencies that ensure the dynamical stability. The thermal stability is also confirmed by the molecular dynamics simulations at 300 K, with negligible changes in the potential energy and the bond length. The selected nanodots have a hexagonal structure with armchair terminations. Two cases of edge termination are considered: the pristine edges and the edges passivated with sulfur atoms. The pristine quantum dots have energy gaps ranging from 2.6 eV to 3 eV, with the highest energy gap observed in MoS_2. The partial density of states shows that the highest occupied and lowest unoccupied molecular orbitals in the pristine case are mainly contributed by the transition metals at the edges. After edge passivation with sulfur atoms, the energy gap significantly decreases in MoS_2 and WS_2, with low-energy orbitals mainly contributed by the passivating S-atoms. The new energy gaps after sulfuration are 1.85 and 0.75 eV for MoS_2 and WS_2 quantum dots, respectively. The energy gap of NbS_2 does not decrease by passivation, which could be a result of the spin doublet state that widens the spin-up and spin-down energy gaps. The change in the free energy of HER shows that the sulfur atoms of MoS_2 that are close to the edges have the highest catalytic performance toward hydrogen evolution with a free energy change of ~0.007 eV. On the unpassivated edges, the change in free energy is much

higher than on the surface due to the strong interaction between H atoms and edge Mo or S atoms. The suitable electronic properties that can be further controlled by edge sulfuration, in addition to the very low change in the free energy for hydrogen evolution, render MoS_2 quantum dots promising for building efficient catalysts.

Author Contributions: Conceptualization, H.A.; data curation, O.H.A.-E. and H.A.; formal analysis, O.H.A.-E.; funding acquisition, O.H.A.-E. and Q.Z.; investigation, O.H.A.-E. and H.A.; methodology, O.H.A.-E. and H.A.; project administration, O.H.A.-E. and H.A.; resources, M.A.S.S.; software, Q.Z.; supervision, A.A.S. and Q.Z.; validation, H.A. and M.A.S.S.; visualization, H.A. and A.A.S.; writing—original draft, O.H.A.-E., H.A. and M.A.S.S.; writing—review and editing, O.H.A.-E. and Q.Z. All authors have read and agreed to the published version of the manuscript.

Funding: This work is supported by the National Natural Science Foundation of China (No. 12274361), the Natural Science Foundation of Jiangsu Province (BK20211361), and the College Natural Science Research Project of Jiangsu Province (20KJA430004). This work is also supported by researchers supporting project number RSP2023R468, King Saud University, Riyadh, Saudi Arabia.

Data Availability Statement: All data generated or analyzed during this study are included in this published article.

Conflicts of Interest: There is no conflict of interest to declare.

Appendix A

The IR spectra of the considered transition metal dichalcogenides quantum dots show that all the vibrational frequencies are real (no imaginary frequencies), which insures the geometrical stability of the structures.

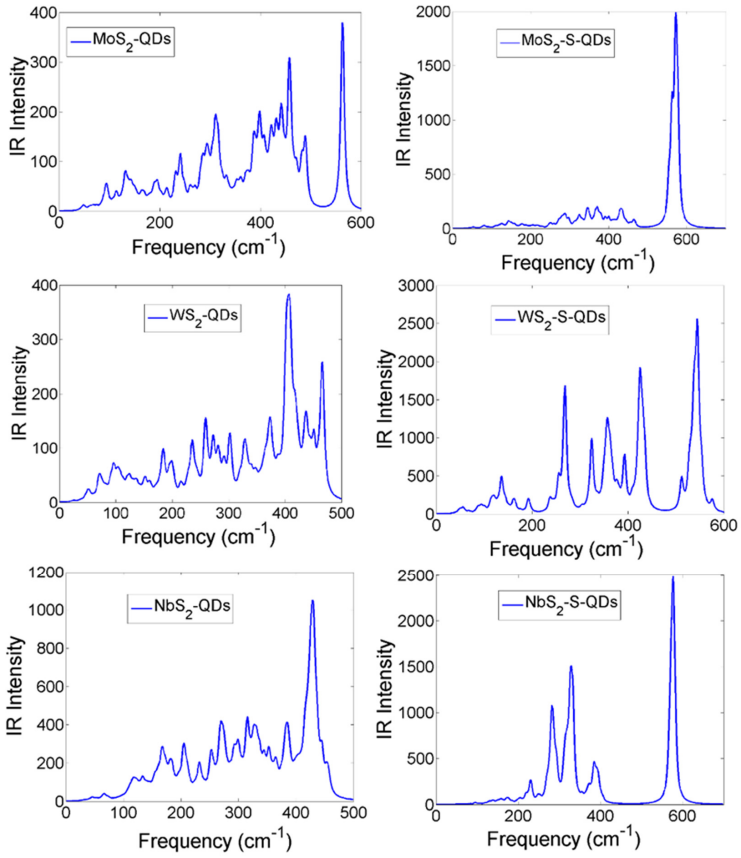


Figure A1. Infrared (IR) spectra of MoS_2, WS_2, and NbS_2 with and without edge passivation with sulfur.

Appendix B

Here, the ab initio molecular dynamics simulations at 300 K for the selected transition metal.

Dichalcogenide quantum dots are presented in Figures A2 and A3. The trajectories in the figures show the time evolution of the potential energy and selected bond lengths at 300 K for 5 femtoseconds. The changes in potential energy and bond length are very small, which indicates that the considered systems are thermally stable at 300 K.

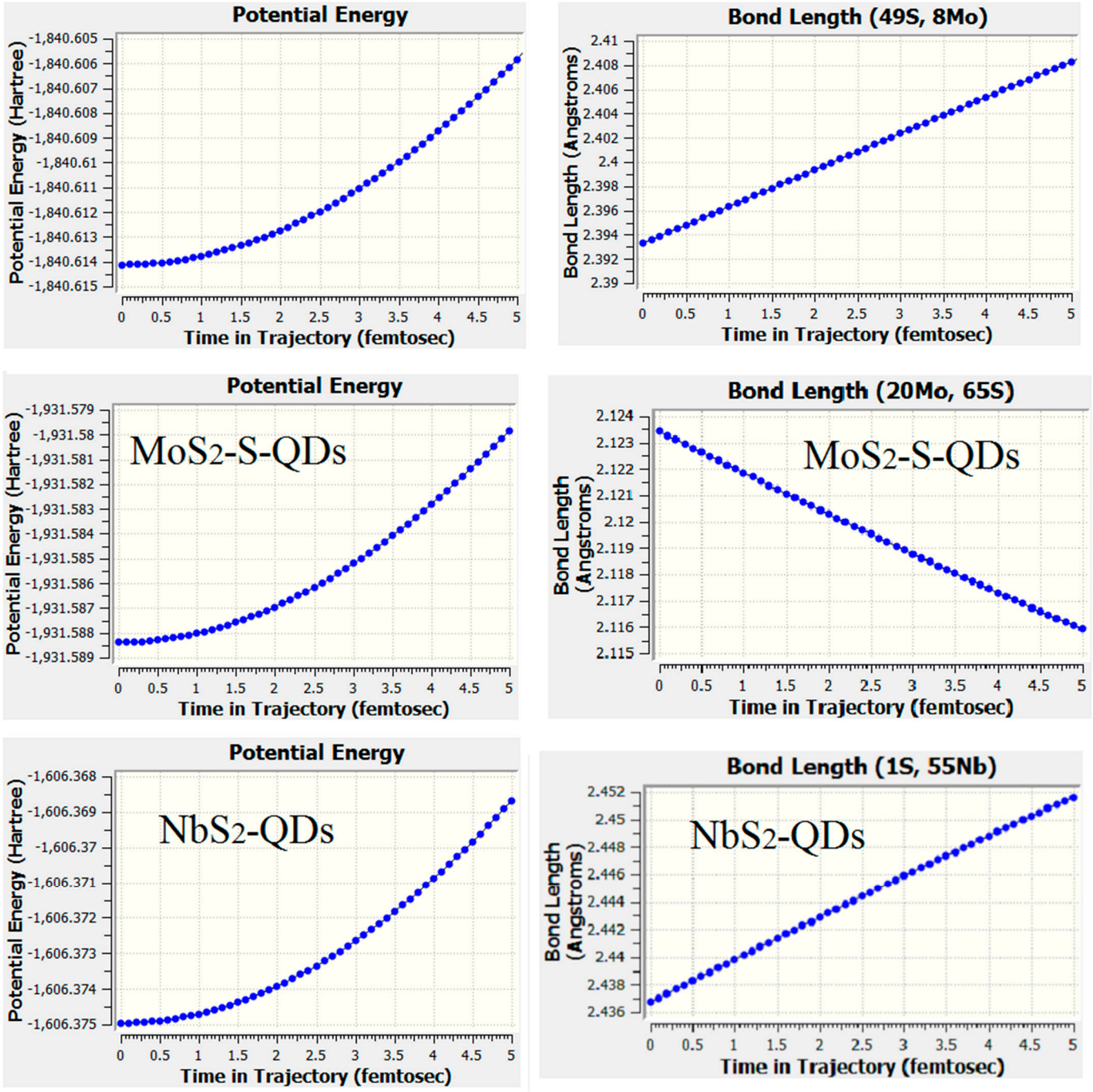


Figure A2. The time evolution of the potential energy and selected Mo−S bond lengths at 300 K for MoS_2, MoS_2−S, and NbS_2 quantum dots.

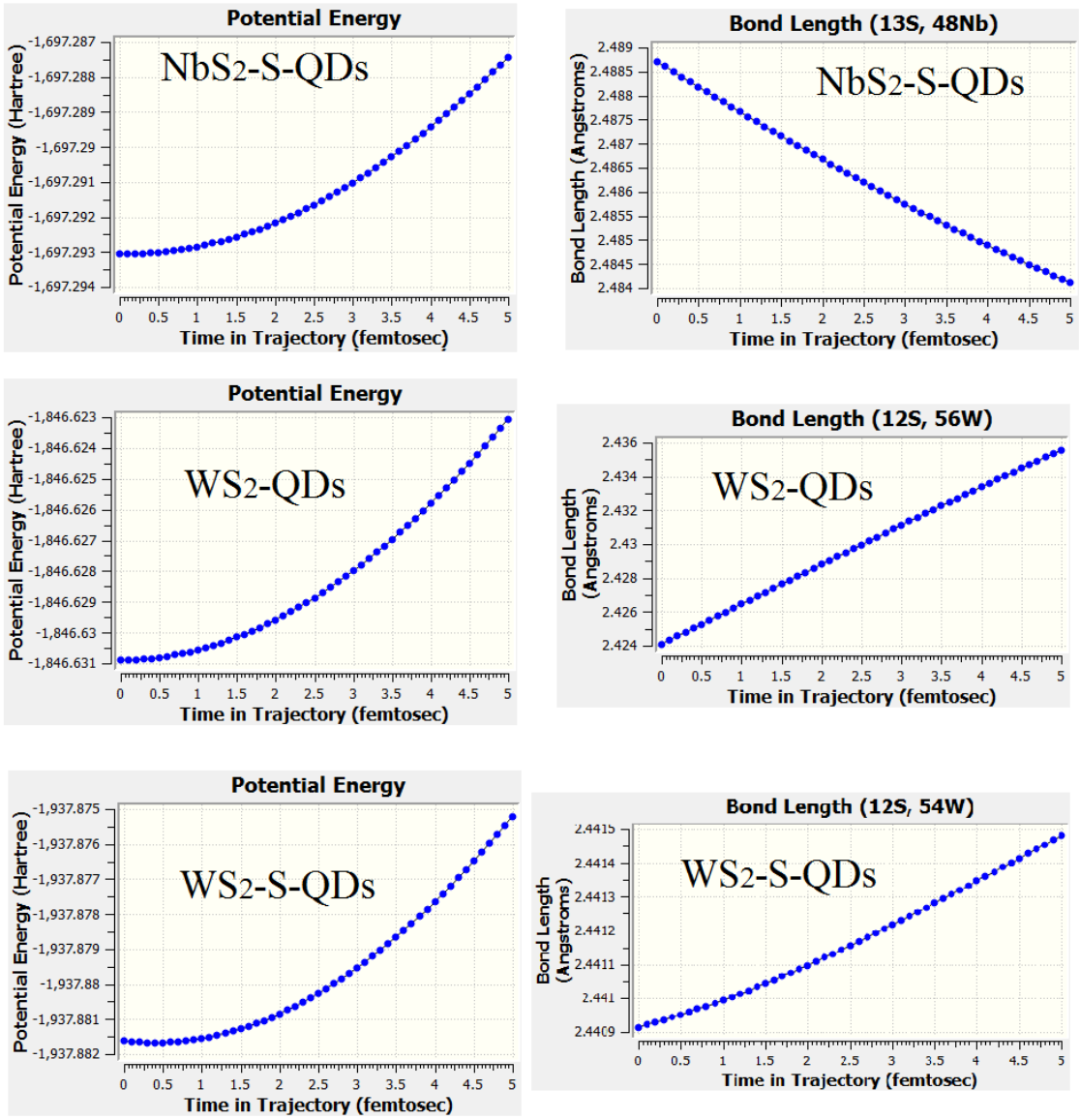


Figure A3. The same as in Figure A2 but for NbS_2-S, WS_2, and WS_2-S quantum dots.

References

1. Chang, C.; Chen, W.; Chen, Y.; Chen, Y.; Chen, Y.; Ding, F.; Fan, C.; Fan, H.J.; Fan, Z.; Gong, C. Recent progress on two-dimensional materials. *Acta Phys.-Chim. Sin* **2021**, *37*, 2108017. [CrossRef]
2. Fiori, G.; Bonaccorso, F.; Iannaccone, G.; Palacios, T.; Neumaier, D.; Seabaugh, A.; Banerjee, S.K.; Colombo, L. Electronics based on two-dimensional materials. *Nat. Nanotechnol.* **2014**, *9*, 768–779. [CrossRef] [PubMed]
3. Chia, X.; Pumera, M. Characteristics and performance of two-dimensional materials for electrocatalysis. *Nat. Catal.* **2018**, *1*, 909–921. [CrossRef]
4. Chen, X.; Yu, H.; Gao, Y.; Wang, L.; Wang, G. The marriage of two-dimensional materials and phase change materials for energy storage, conversion and applications. *EnergyChem* **2022**, *4*, 100071. [CrossRef]
5. Zhang, X.; Hou, L.; Ciesielski, A.; Samorì, P. 2D materials beyond graphene for high-performance energy storage applications. *Adv. Energy Mater.* **2016**, *6*, 1600671. [CrossRef]
6. Das, S.; Pandey, D.; Thomas, J.; Roy, T. The role of graphene and other 2D materials in solar photovoltaics. *Adv. Mater.* **2019**, *31*, 1802722. [CrossRef] [PubMed]
7. Abdelsalam, H.; Atta, M.M.; Osman, W.; Zhang, Q. Two-dimensional quantum dots for highly efficient heterojunction solar cells. *J. Colloid Interface Sci.* **2021**, *603*, 48–57. [CrossRef]
8. Iannaccone, G.; Bonaccorso, F.; Colombo, L.; Fiori, G. Quantum engineering of transistors based on 2D materials heterostructures. *Nat. Nanotechnol.* **2018**, *13*, 183–191. [CrossRef] [PubMed]
9. Yang, H.; Valenzuela, S.O.; Chshiev, M.; Couet, S.; Dieny, B.; Dlubak, B.; Fert, A.; Garello, K.; Jamet, M.; Jeong, D.-E. Two-dimensional materials prospects for non-volatile spintronic memories. *Nature* **2022**, *606*, 663–673. [CrossRef] [PubMed]

10. Abdelsalam, H.; Atta, M.M.; Saroka, V.A.; Zhang, Q. Anomalous magnetic and transport properties of laterally connected graphene quantum dots. *J. Mater. Sci.* **2022**, *57*, 14356–14370. [CrossRef]
11. Yang, S.; Jiang, C.; Wei, S.-h. Gas sensing in 2D materials. *Appl. Phys. Rev.* **2017**, *4*, 021304. [CrossRef]
12. Abdelsalam, H.; Saroka, V.A.; Atta, M.M.; Abd-Elkader, O.H.; Zaghloul, N.S.; Zhang, Q. Tunable Sensing and Transport Properties of Doped Hexagonal Boron Nitride Quantum Dots for Efficient Gas Sensors. *Crystals* **2022**, *12*, 1684. [CrossRef]
13. Rasool, K.; Pandey, R.P.; Rasheed, P.A.; Buczek, S.; Gogotsi, Y.; Mahmoud, K.A. Water treatment and environmental remediation applications of two-dimensional metal carbides (MXenes). *Mater. Today* **2019**, *30*, 80–102. [CrossRef]
14. Saad, M.A.; Sakr, M.A.; Saroka, V.A.; Abdelsalam, H. Chemically modified covalent organic frameworks for a healthy and sustainable environment: First-principles study. *Chemosphere* **2022**, *308*, 136581. [CrossRef] [PubMed]
15. Raza, A.; Hassan, J.Z.; Mahmood, A.; Nabgan, W.; Ikram, M. Recent advances in membrane-enabled water desalination by 2D frameworks: Graphene and beyond. *Desalination* **2022**, *531*, 115684. [CrossRef]
16. Tang, T.; Li, S.; Sun, J.; Wang, Z.; Guan, J. Advances and challenges in two-dimensional materials for oxygen evolution. *Nano Res.* **2022**, *15*, 8714–8750. [CrossRef]
17. Hasani, A.; Tekalgne, M.; Van Le, Q.; Jang, H.W.; Kim, S.Y. Two-dimensional materials as catalysts for solar fuels: Hydrogen evolution reaction and CO_2 reduction. *J. Mater. Chem. A* **2019**, *7*, 430–454. [CrossRef]
18. Claassen, M.; Xian, L.; Kennes, D.M.; Rubio, A. Ultra-strong spin–orbit coupling and topological moiré engineering in twisted ZrS2 bilayers. *Nat. Commun.* **2022**, *13*, 1–8. [CrossRef]
19. Wakamura, T.; Reale, F.; Palczynski, P.; Zhao, M.; Johnson, A.; Guéron, S.; Mattevi, C.; Ouerghi, A.; Bouchiat, H. Spin-orbit interaction induced in graphene by transition metal dichalcogenides. *Phys. Rev. B* **2019**, *99*, 245402. [CrossRef]
20. Kalantar-zadeh, K.; Ou, J.Z.; Daeneke, T.; Strano, M.S.; Pumera, M.; Gras, S.L. Two-dimensional transition metal dichalcogenides in biosystems. *Adv. Funct. Mater.* **2015**, *25*, 5086–5099. [CrossRef]
21. Kozawa, D.; Kumar, R.; Carvalho, A.; Kumar Amara, K.; Zhao, W.; Wang, S.; Toh, M.; Ribeiro, R.M.; Castro Neto, A.H.; Matsuda, K. Photocarrier relaxation pathway in two-dimensional semiconducting transition metal dichalcogenides. *Nat. Commun.* **2014**, *5*, 1–7. [CrossRef]
22. Bernardi, M.; Palummo, M.; Grossman, J.C. Extraordinary sunlight absorption and one nanometer thick photovoltaics using two-dimensional monolayer materials. *Nano Lett.* **2013**, *13*, 3664–3670. [CrossRef] [PubMed]
23. Amani, M.; Lien, D.-H.; Kiriya, D.; Xiao, J.; Azcatl, A.; Noh, J.; Madhvapathy, S.R.; Addou, R.; Kc, S.; Dubey, M. Near-unity photoluminescence quantum yield in MoS_2. *Science* **2015**, *350*, 1065–1068. [CrossRef] [PubMed]
24. Gutiérrez, H.R.; Perea-López, N.; Elías, A.L.; Berkdemir, A.; Wang, B.; Lv, R.; López-Urías, F.; Crespi, V.H.; Terrones, H.; Terrones, M. Extraordinary room-temperature photoluminescence in triangular WS_2 monolayers. *Nano Lett.* **2013**, *13*, 3447–3454. [CrossRef] [PubMed]
25. Radisavljevic, B.; Radenovic, A.; Brivio, J.; Giacometti, V.; Kis, A. Single-layer MoS_2 transistors. *Nat. Nanotechnol.* **2011**, *6*, 147–150. [CrossRef]
26. Wu, F.; Tian, H.; Shen, Y.; Hou, Z.; Ren, J.; Gou, G.; Sun, Y.; Yang, Y.; Ren, T.-L. Vertical MoS_2 transistors with sub-1-nm gate lengths. *Nature* **2022**, *603*, 259–264. [CrossRef]
27. Niu, S.; Cai, J.; Wang, G. Two-dimensional MoS_2 for hydrogen evolution reaction catalysis: The electronic structure regulation. *Nano Res.* **2021**, *14*, 1985–2002. [CrossRef]
28. Sun, Z.; He, J.; Yuan, M.; Lin, L.; Zhang, Z.; Kang, Z.; Liao, Q.; Li, H.; Sun, G.; Yang, X. Li^+-clipping for edge S-vacancy MoS_2 quantum dots as an efficient bifunctional electrocatalyst enabling discharge growth of amorphous Li_2O_2 film. *Nano Energy* **2019**, *65*, 103996. [CrossRef]
29. Mohanty, B.; Ghorbani-Asl, M.; Kretschmer, S.; Ghosh, A.; Guha, P.; Panda, S.K.; Jena, B.; Krasheninnikov, A.V.; Jena, B.K. MoS_2 quantum dots as efficient catalyst materials for the oxygen evolution reaction. *Acs Catal.* **2018**, *8*, 1683–1689. [CrossRef]
30. Theibault, M.; Chandler, C.; Dabo, I.; Abruna, H.D. Transition Metal Dichalcogenides as Effective Catalysts for High-Rate Lithium–Sulfur Batteries. *ACS Catal.* **2023**, *13*, 3684–3691. [CrossRef]
31. Mondal, A.; Vomiero, A. 2D Transition Metal Dichalcogenides-Based Electrocatalysts for Hydrogen Evolution Reaction. *Adv. Funct. Mater.* **2022**, *32*, 2208994. [CrossRef]
32. Tian, L.; Qiao, H.; Huang, Z.; Qi, X. Li-Ion Intercalated Exfoliated WS_2 Nanosheets with Enhanced Electrocatalytic Hydrogen Evolution Performance. *Cryst. Res. Technol.* **2021**, *56*, 2000165. [CrossRef]
33. Gan, X.; Lei, D.; Ye, R.; Zhao, H.; Wong, K.-Y. Transition metal dichalcogenide-based mixed-dimensional heterostructures for visible-light-driven photocatalysis: Dimensionality and interface engineering. *Nano Res.* **2021**, *14*, 2003–2022. [CrossRef]
34. Ran, J.; Zhang, J.; Yu, J.; Jaroniec, M.; Qiao, S.Z. Earth-abundant cocatalysts for semiconductor-based photocatalytic water splitting. *Chem. Soc. Rev.* **2014**, *43*, 7787–7812. [CrossRef]
35. Fadojutimi, P.O.; Gqoba, S.S.; Tetana, Z.N.; Moma, J. Transition Metal Dichalcogenides [MX_2] in Photocatalytic Water Splitting. *Catalysts* **2022**, *12*, 468. [CrossRef]
36. Hinnemann, B.; Moses, P.G.; Bonde, J.; Jørgensen, K.P.; Nielsen, J.H.; Horch, S.; Chorkendorff, I.; Nørskov, J.K. Biomimetic hydrogen evolution: MoS_2 nanoparticles as catalyst for hydrogen evolution. *J. Am. Chem. Soc.* **2005**, *127*, 5308–5309. [CrossRef]
37. Li, Y.; Wang, H.; Xie, L.; Liang, Y.; Hong, G.; Dai, H. MoS_2 nanoparticles grown on graphene: An advanced catalyst for the hydrogen evolution reaction. *J. Am. Chem. Soc.* **2011**, *133*, 7296–7299. [CrossRef]

38. Li, G.; Zhang, D.; Qiao, Q.; Yu, Y.; Peterson, D.; Zafar, A.; Kumar, R.; Curtarolo, S.; Hunte, F.; Shannon, S. All the catalytic active sites of MoS_2 for hydrogen evolution. *J. Am. Chem. Soc.* **2016**, *138*, 16632–16638. [CrossRef]
39. Saroka, V.; Lukyanchuk, I.; Portnoi, M.; Abdelsalam, H. Electro-optical properties of phosphorene quantum dots. *Phys. Rev. B* **2017**, *96*, 085436. [CrossRef]
40. Osman, W.; Saad, M.; Ibrahim, M.; Yahia, I.; Abdelsalam, H.; Zhang, Q. Electronic, optical, and catalytic properties of finite antimonene nanoribbons: First principles study. *Phys. Scr.* **2022**, *97*, 035802. [CrossRef]
41. Wang, X.; Sun, G.; Li, N.; Chen, P. Quantum dots derived from two-dimensional materials and their applications for catalysis and energy. *Chem. Soc. Rev.* **2016**, *45*, 2239–2262. [CrossRef] [PubMed]
42. Abdelsalam, H.; Zhang, Q.F. Properties and applications of quantum dots derived from two-dimensional materials. *Adv. Phys. X* **2022**, *7*, 2048966. [CrossRef]
43. Jaramillo, T.F.; Jørgensen, K.P.; Bonde, J.; Nielsen, J.H.; Horch, S.; Chorkendorff, I. Identification of active edge sites for electrochemical H2 evolution from MoS_2 nanocatalysts. *Science* **2007**, *317*, 100–102. [CrossRef] [PubMed]
44. Chen, J.; Liu, G.; Zhu, Y.-z.; Su, M.; Yin, P.; Wu, X.-j.; Lu, Q.; Tan, C.; Zhao, M.; Liu, Z. Ag@MoS_2 core–shell heterostructure as SERS platform to reveal the hydrogen evolution active sites of single-layer MoS_2. *J. Am. Chem. Soc.* **2020**, *142*, 7161–7167. [CrossRef]
45. Mohanty, B.; Mitra, A.; Jena, B.; Jena, B.K. MoS_2 quantum dots as efficient electrocatalyst for hydrogen evolution reaction over a wide pH range. *Energy Fuels* **2020**, *34*, 10268–10275. [CrossRef]
46. Liu, M.; Zhang, C.; Han, A.; Wang, L.; Sun, Y.; Zhu, C.; Li, R.; Ye, S. Modulation of morphology and electronic structure on MoS_2-based electrocatalysts for water splitting. *Nano Res.* **2022**, *15*, 6862–6887. [CrossRef]
47. Chen, B.; Hu, P.; Yang, F.; Hua, X.; Yang, F.F.; Zhu, F.; Sun, R.; Hao, K.; Wang, K.; Yin, Z. In situ porousized MoS_2 nano islands enhance HER/OER bifunctional electrocatalysis. *Small* **2023**, *19*, e2207177. [CrossRef]
48. Hu, J.; Yu, L.; Deng, J.; Wang, Y.; Cheng, K.; Ma, C.; Zhang, Q.; Wen, W.; Yu, S.; Pan, Y. Sulfur vacancy-rich MoS_2 as a catalyst for the hydrogenation of CO2 to methanol. *Nat. Catal.* **2021**, *4*, 242–250. [CrossRef]
49. Shen, S.; Hu, Z.; Zhang, H.; Song, K.; Wang, Z.; Lin, Z.; Zhang, Q.; Gu, L.; Zhong, W. Highly active Si sites enabled by negative valent Ru for electrocatalytic hydrogen evolution in LaRuSi. *Angew. Chem.* **2022**, *134*, e202206460. [CrossRef]
50. Wang, D.; Wu, J.; Jiao, L.; Xie, L. In situ identification of active sites during electrocatalytic hydrogen evolution. *Nano Res.* **2023**, 1–9. [CrossRef]
51. Gopalakrishnan, D.; Damien, D.; Shaijumon, M.M. MoS_2 quantum dot-interspersed exfoliated MoS_2 nanosheets. *ACS Nano* **2014**, *8*, 5297–5303. [CrossRef] [PubMed]
52. Yang, R.; Fan, Y.; Mei, L.; Shin, H.S.; Voiry, D.; Lu, Q.; Li, J.; Zeng, Z. Synthesis of atomically thin sheets by the intercalation-based exfoliation of layered materials. *Nat. Synth.* **2023**, *2*, 101–118. [CrossRef]
53. Ohta, N.; Mehata, M.S. In situ synthesis of WS_2 QDs for sensing of H2O2: Quenching and recovery of absorption and photoluminescence. *Mater. Today Commun.* **2023**, *34*, 105013.
54. Ahn, C.; Lim, H. Synthesis of monolayer 2D MoS_2 quantum dots and nanomesh films by inorganic molecular chemical vapor deposition for quantum confinement effect control. *Bull. Korean Chem. Soc.* **2022**, *43*, 1184–1190. [CrossRef]
55. Zhou, L.; Yan, S.; Wu, H.; Song, H.; Shi, Y. Facile sonication synthesis of WS_2 quantum dots for photoelectrochemical performance. *Catalysts* **2017**, *7*, 18. [CrossRef]
56. Pourmadadi, M.; Tajiki, A.; Hosseini, S.M.; Samadi, A.; Abdouss, M.; Daneshnia, S.; Yazdian, F. A comprehensive review of synthesis, structure, properties, and functionalization of MoS_2; emphasis on drug delivery, photothermal therapy, and tissue engineering applications. *J. Drug Deliv. Sci. Technol.* **2022**, *76*, 103767. [CrossRef]
57. Sideri, I.K.; Arenal, R.; Tagmatarchis, N. Covalently functionalized MoS_2 with dithiolenes. *ACS Mater. Lett.* **2020**, *2*, 832–837. [CrossRef]
58. Tadi, K.K.; Palve, A.M.; Pal, S.; Sudeep, P.; Narayanan, T.N. Single step, bulk synthesis of engineered MoS_2 quantum dots for multifunctional electrocatalysis. *Nanotechnology* **2016**, *27*, 275402. [CrossRef]
59. Frisch, M.J.; Trucks, G.W.; Schlegel, H.B.; Scuseria, G.E.; Robb, M.A.; Cheeseman, J.R.; Scalmani, G.; Barone, V.; Petersson, G.A.; Nakatsuji, H.; et al. *Gaussian 16 Rev. C.01*; Gaussian Inc.: Wallingford, CT, USA, 2016.
60. Zhao, Y.; Truhlar, D.G. The M06 suite of density functionals for main group thermochemistry, thermochemical kinetics, noncovalent interactions, excited states, and transition elements: Two new functionals and systematic testing of four M06-class functionals and 12 other functionals. *Theor. Chem. Acc.* **2008**, *120*, 215–241.
61. Abd Elkodous, M.; El-Khawaga, A.M.; Maksoud, M.A.; El-Sayyad, G.S.; Alias, N.; Abdelsalam, H.; Ibrahim, M.A.; Elsayed, M.A.; Kawamura, G.; Lockman, Z. Enhanced photocatalytic and antimicrobial performance of a multifunctional Cu-loaded nanocomposite under UV light: Theoretical and experimental study. *Nanoscale* **2022**, *14*, 8306–8317. [CrossRef]
62. Hay, P.J.; Wadt, W.R. Ab initio effective core potentials for molecular calculations. Potentials for the transition metal atoms Sc to Hg. *J. Chem. Phys.* **1985**, *82*, 270–283. [CrossRef]
63. Abdelsalam, H.; Teleb, N.; Wang, B.; Yunoki, S.; Zhang, Q. The electronic, adsorption, and catalytic properties of Bi-, Sb-, and As-nanoclusters. *Catal. Today* **2021**, *376*, 126–133. [CrossRef]
64. Iyengar, S.S.; Schlegel, H.B.; Millam, J.M.A.; Voth, G.; Scuseria, G.E.; Frisch, M.J. Ab initio molecular dynamics: Propagating the density matrix with Gaussian orbitals. II. Generalizations based on mass-weighting, idempotency, energy conservation and choice of initial conditions. *J. Chem. Phys.* **2001**, *115*, 10291–10302. [CrossRef]

65. Schlegel, H.B.; Iyengar, S.S.; Li, X.; Millam, J.M.; Voth, G.A.; Scuseria, G.E.; Frisch, M.J. Ab initio molecular dynamics: Propagating the density matrix with Gaussian orbitals. III. Comparison with Born–Oppenheimer dynamics. *J. Chem. Phys.* **2002**, *117*, 8694–8704. [CrossRef]
66. O'boyle, N.M.; Tenderholt, A.L.; Langner, K.M. Cclib: A library for package-independent computational chemistry algorithms. *J. Comput. Chem.* **2008**, *29*, 839–845. [CrossRef]
67. Ito, Y.; Cong, W.; Fujita, T.; Tang, Z.; Chen, M. High catalytic activity of nitrogen and sulfur co-doped nanoporous graphene in the hydrogen evolution reaction. *Angew. Chem.* **2015**, *127*, 2159–2164. [CrossRef]
68. Abdelsalam, H.; Younis, W.; Saroka, V.; Teleb, N.; Yunoki, S.; Zhang, Q. Interaction of hydrated metals with chemically modified hexagonal boron nitride quantum dots: Wastewater treatment and water splitting. *Phys. Chem. Chem. Phys.* **2020**, *22*, 2566–2579. [CrossRef]
69. Jiao, Y.; Zheng, Y.; Davey, K.; Qiao, S.-Z. Activity origin and catalyst design principles for electrocatalytic hydrogen evolution on heteroatom-doped graphene. *Nat. Energy* **2016**, *1*, 16130. [CrossRef]
70. Zheng, Y.; Jiao, Y.; Zhu, Y.; Li, L.; Han, Y.; Chen, Y.; Du, A.; Jaroniec, M.; Qiao, S. Hydrogen evolution by a metal-free electrocatalyst. *Nat. Commun.* **2014**, *5*, 3783. [CrossRef]

Disclaimer/Publisher's Note: The statements, opinions and data contained in all publications are solely those of the individual author(s) and contributor(s) and not of MDPI and/or the editor(s). MDPI and/or the editor(s) disclaim responsibility for any injury to people or property resulting from any ideas, methods, instructions or products referred to in the content.